Colloid thruster droplet evolution analysis using molecular dynamics

IEPC-2017-66

Presented at the 35th International Electric Propulsion Conference
Georgia Institute of Technology – Atlanta, Georgia – USA
October 8–12, 2017
Neil Mehta* and Deborah A. Levin†
University of Illinois, Urbana-Champaign, Illinois, 61801, USA

We have used molecular dynamics as a predictive tool to study the disintegration of large droplet emitted during the electrospray process. We consider an isolated droplet of 1-ethyl-3-methylimidazolium Tetrafluoroborate (EMIM-BF_4) as a test case to understand the effects of normal and radial electric fields on the final mass, volume, and charge of the droplet. The disintegration process was not found to be continuous but occurred spontaneously during the initial time steps for the range of normal and radial electric fields used in this work. Increasing the field strengths led to decrease in the emission of secondary droplets and larger aggregates but increased the emission of smaller species. The volume decay rate of the primary droplet was found to depend linearly on the normal and radial electric field strengths. The radii of the ion aggregates emitted from the primary droplet and the emission break-up times agreed well with those from the Rayleigh instability theory and the Coulomb fission model.

*PhD Candidate, Department of Aerospace Engineering, and namehta4@illinois.edu
†Professor, Department of Aerospace Engineering, and deblevin@illinois.edu

Nomenclature

ϕ_l = potential obtained from the solution to Laplace's equation
Q_i = Partial charges on CG site i
r_{ij} = distance between CG site i and j
R_c = Coulomb interaction cut-off radius
p = volume decay rate
z = number of charges
ϵ_0 = permittivity of vacuum
γ = Surface tension
r = radius of the primary droplet
e = elementary charge
E_s = electric field associated with the number of charges
E_{R_y} = electric field required to generate Rayleigh instabilities
R_B = Born radius
R_s = secondary droplet radius
t_{break} = break-up time of the jet
α_m = jet growth rate
σ = surface charge density
I = surface current
ρ = mass density
ϵ = Dielectric permittivity

I. Introduction

Rapid developments in the field of electronic and manufacturing miniaturization has resulted in an uncapped growth of nanosatellites. Nano-satellites have the potential to be used for remote sensing of agricultural lands,[1] earth-imaging,[2] and to create constellations for low data rate communications.[3] These satellites typically weigh between 1 - 10 kg (2.2 - 22 lb) and have severe volumetric and weight constraints. As a part of a larger cluster, these nano-satellites often require an on-board propulsion device for maintaining their altitude and for orbit correction maneuvers. Electric propulsion offers a lucrative solution in the form of multiple propulsion systems, each suitable for a particular mission requirement. Electric propulsion devices, such as ion and Hall-effect thrusters are competent but are complex and require ion bombardment sources, electromagnets, and many other sub-systems, such as, the electrodes, accelerator grids, and a hollow cathode assembly.[4] These complexities marginally add to the weight of the satellite, which may not be problem for moderate or small sized satellites but is an important consideration on nano-satellites.

For nano-satellites, a subset of electrostatic propulsion device known as field emission electric propulsion (FEEP)[5] or Colloid thrusters can be used. These devices use conducting liquids as propellants, such that,when a capillary fed by this conducting liquid in the presence of an external electric field, a fine jet of ions is emitted from a Taylor[6] cone formed at the head of the capillary and the emitted ions are further accelerated by the electric field. The emission from the Taylor cone is also known as an electrospray and its applications are not just limited to FEEP thrusters. Electrosprays have been used extensively in the field of micro fabrication because the electrosprays allow for controlled deposition[7] for applications involving microfilm deposition,[8] microcircuit manufacturing,[9] and ion beam lithography.[10] The electrosprays of charged liquids also find applications in the fields such as biomedical engineering,[11,12] especially in the analysis of biological tissues,[13] biomedical engineering,[11,12] microelectromechanical systems (MEMS), pharmaceutical development,[14,15] food sciences,[16] and industrial engineering.[17,18]

While FEEP devices use liquid metal based propellants, colloid thrusters use relatively benign non-metallic ionic liquids, which, similar to liquid cesium exhibit the formation of Taylor cone in the presence of an external electric field. Ionic liquids (ILs) are defined as salts having a melting point less than room temperature (373 K) and similar to liquid cesium, have the ability to form a Taylor cone and emit ions. ILs are used as propellants in colloid thrusters with the advantage of producing higher thrust-to-power ratios compared to the traditional liquid cesium based FEEP[19] thrusters. Depending on the operation mode, ionic liquids breakdown into either into individual ion species or sub-micron sized droplets (colloids) that are accelerated by the electric fields, generating high exhaust velocities. The performance and operability of colloid thrusters has been tested in space on the NASA ST-7 LISA Pathfinder mission.[20,21]

A large number of ionic liquids can be used as propellants for electrosprays,[22,23] to cater to the wide range of performance requirements. Therefore, it is necessary to have experimental and simulation based ability to predict the thrust, required voltages, and mode of operation to design electrospray devices. Molecular dynamics (MD) is a particle based method that allows us to understand the nature of electrosprays at an atomistic level.[24] The availability of large number of inter-atomic potentials makes it possible to model virtually any of the ILs. Although, MD is a mature computational technique, it becomes computational expensive to

model the electrospray simulations. MD simulations scale on the order of $O(N^2)$, where, N is the number of atoms, making them very expensive to model large simulations ($>$ 10,000 atoms). Researchers such as, Borner, *et al.*,[25] have overcome this problem by using the coarse-grained potentials to model electrospray simulations of 1-ethyl-3-methylimidazolium Tetrafluoroborate (EMIM-BF_4). The coarse-grained potential of EMIM-BF_4 was obtained by modifying the CG potential of EMIM-NO_3 derived by Wang, *et al.*[26–28] from the all-atom potential using the effective field coarse graining (EFCG) method.

Colloid thruster experiments provide important information regarding the species specific emission currents[29] and the thrust generated for the applied potential across the device, but, they lack the specificities of the shape and strength of the electric field generated around the mouth of the capillary. It should also be noted that while the experiments are conducted over length and time scales of micro-meters and micro-seconds, the current computational capability only allows one to simulate electrosprays at length and timescales of nano-meters and nano-seconds. Thus, it becomes incumbent for the MD simulations to use external boundary conditions that recreate the Taylor cone formation and emission characteristics similar to the experiments without the knowledge of the spatial and temporal evolution of the electric fields generated during the experiments, which are discussed in detail in our previous published work.[30]

Electrospray experiments and simulations have been performed to either study the formation of Taylor cone[31,32] or to obtain the final emission currents, our knowledge of what happens to the emitted species when traveling between the Taylor cone and the extractor plane is limited and often contested.[33] Many studies have been performed to analyze the mechanism of charged droplet disintegration[34] which occurs due to the disproportionate and asymmetric charge density. A variety of techniques, which include, high speed photography,[35,36] rapid solidification using sol-gel,[37] and MD simulations[38,39] have been used to capture the transient behavior of the ion aggregates emitted by the electrosprays. While the shape deformation[40] and mass loss can be analyzed using experimental[41] methods, only theoretical models and MD simulations are capable of providing insight regarding charge reduction during the droplet disintegration process. Leading theories for charged droplet disintegration include the charged residue mechanism (CRM),[42] which states that smaller ions are emitted by the original droplet due to successive instabilities predicted by the Rayleigh theory[43] and the ion evaporation mechanism (IEM),[44] which describes the disintegration process using first order reaction kinetics. Both theories are valid in their respective limits but their applicability to a given droplet disintegration process is not well understood.[45] MD simulations allow the study of droplet disintegration for any IL and obtain detailed information regarding the emitted species, velocities, charges, etc.

Previous MD simulations have been performed for a system of water molecules charged by Cl-[38] and pronated diglycine molecules[39] to study the effect of Rayleigh critical limit and the evolution of nanojet from the droplets. Simulations in this work are aimed at understanding the effects of electric field strengths on the droplet disintegration using EMIM-BF_4. The boundary conditions and the domain information used for the MD simulations are first discussed in Sec. II. The formation of Taylor cone and the evolution of the charged droplet in th applied electric fields are discussed using MD snapshots in Sec. III A and B, respectively. The effect of normal and radial electric fields on the mass and volume of the droplet are discussed in Sec. III C. Finally, the droplet radii and charges obtained from the MD simulations are compared with the theoretical models in Sec. III D.

II. Problem set-up and numerical parameters used for electrospray MD simulations

A. Preparing the electrospray MD simulation system

Since a large number of molecules are required to simulate non-equilibrium processes such as electrosprays in MD, we have used coarse graining techniques to reduce the computational cost. Wang, *et al.*,[27] have suggested the use of Effective Field Coarse Graining (EFCG)[26] method which works on the principle of simplifying non-essential group of atoms and their respective degrees-of-freedom as a single coarse-grained site.[28] Wang, *et al.*[26] have reduced the non-essential degrees-of-freedom in the EMIM-NO_3 ion-pairs. Using CG, the number of required particles to simulate one molecule was reduced from 27 atoms to just five CG sites. The same CG potential was modified by replacing the anion from NO_3 to BF_4 to obtain the CG potential for EMIM-BF_4. The two CH_3 groups were simplified to two single sites 'M1' and 'M2' respectively. The largest computational saving is observed by reducing the large imidizolium group to a single CG site. The CH_2 group in the cation and the BF_4 anion were simplified to sites 'MR' and 'BF4', respectively. Equilibration and electrospray simulations of CG EMIM-BF_4 were performed for this work using the potential derived by Wang, *et al.*[27] Borner, *et al.*,[25] also modeled the electrical conductivity of CG EMIM-BF_4 in MD simulations and found good agreement with the experimental values. Details regarding the coarse-graining procedure has been published previously.[46]

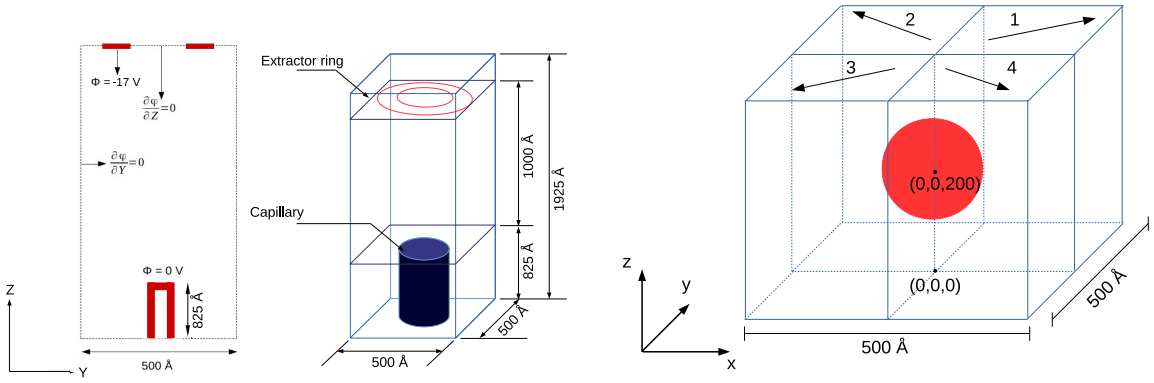

(a) Electrical boundary conditions.

(b) Schematic of isolated droplet simulation.

Figure 1. Schematic of an MD electrospray simulation and isolated droplet simulations and boundary conditions used for extrusion simulations.

The simulations results discussed in this paper were performed using the boundary conditions and domain dimensions shown in Fig. 1(a). The extraction voltages used for the EMIM-BF_4 simulation was ϕ = -17 V, as it generates potential gradients comparable to those that occur over the length scale of the experiments. All simulations were performed in LAMMPS using the direct Coulomb (DC) method to calculate all electrostatic non-bonded interactions with a cut-off radius of R_c = 20 Å. The capillary of radius 56 Å and height 825 Å was formed using 49,878 platinum atoms and was filled with 28.365 EMIM-BF_4 ion-pairs for the electrospray simulations. The ion-pairs in the capillary were first energy minimized using the system potential energy as the criteria to remove any non-physical CG site or bond overlaps that may exist. The ion-pairs were them equilibrated to a temperature

of 297 K using the canonical (NVT) ensemble. A repulsive wall was used to generate a mass flow rate of 1.09×10^{-11} through the capillary for the electrospray simulations. The emitted positive ion species were classified based on the number of cations present in the aggregate. Using the definition, $(\mathrm{EMIM-BF_4})_\mathrm{n} \cdot \mathrm{EMIM^+}$, if n was zero, the aggregate was termed a *monomer* and if $n = 1$ or 2, the aggregate was defined as a *dimer* or *trimer*, respectively. Aggregates containing more than $n = 9$ were termed as droplets.

A large droplet emitted from the extrusion simulation was isolated and simulations were performed using this primary droplet to study the evolution of an IL droplet in the presence of an external electric field. The droplet obtained was placed in the center of a domain consisting of four quadrants. The normal electric field, E_z was applied along the Z axis and its strength was constant in all the four quadrants but to model the radial electric field, the polarity of E_x and E_y were modified depending on the quadrant. In all quadrants, both, E_x and E_y were provided constant and equal magnitude. However, while the polarity of both E_x and E_y were positive in the first quadrant, in the second quadrant, the polarity of the E_x was changed to negative. Similarly, the polarity of the both E_x and E_y was negative in the third quadrant and was changed to positive E_x but negative E_y in the fourth quadrant. This effectively allowed us to create radial electric fields that counteract the cohesion of the droplet generated due to the electrostatic forces. The boundaries in X and Y directions were considered non-periodic. The boundaries in the Z direction were 'shrink-wrapped',[47] a feature which allows the domain boundaries to extend during the simulations to encompass all atoms or CG sites, no matter how far they move.

B. Boundary conditions for electrospray simulations

The external electric fields play an important role in determining the emitted ion species and the general shape of the structure of Taylor cone at the mouth of the capillary. The external electric field implemented on the electrospray simulations was calculated using the potential, ϕ_l, derived by solving the Laplace's equation,

$$\nabla^2 \phi_l = 0 \tag{1}$$

The boundary conditions used to solve the Eq. 1 are shown in Fig. 1(a). The entire outer surface of the capillary was grounded using a Dirichlet boundary condition of $\phi = 0$ V. This boundary condition is physically accurate and representative of the experimental set-up used to generate the electrosprays. However, it should be noted that experiments are conducted with capillary diameters and capillary-extractor distances on the order of micro-meters, while the current computational capability allows one to perform MD simulations only on the scale of nano-meters. The simulation domain was non-periodic in all three dimension and a Neumann boundary condition was applied on all three boundaries. Therefore, the total electric potential exerted on the ith CG site would be,

$$\varphi_{tot_i} = C \sum_{\substack{i \neq j \\ r_{ij} < R_c}}^{n} \frac{Q_i Q_j}{r_{ij}} + \varphi_l \tag{2}$$

such that, Q_i and Q_j are the partial charges on the CG sites, n is the total number of CG sites, and $R_c = 20$ Å is the cut-off radius used for the simulations. The first term of Eq. 2 represents the Coulomb interaction potential between the two CG site, while the second

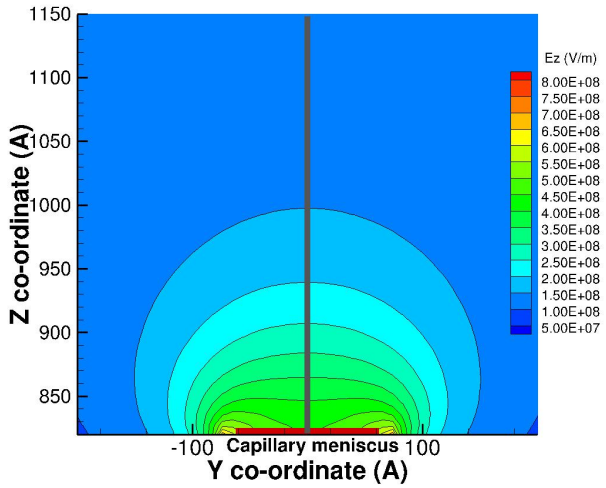

(a) Contour plot of the normal electric field.

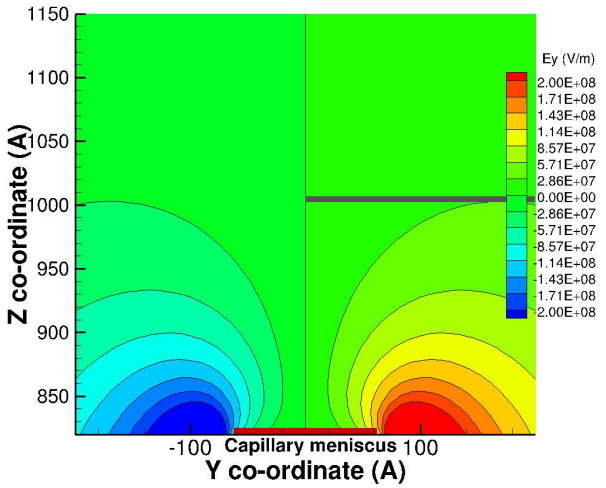

(b) Contour plot of the radial electric field.

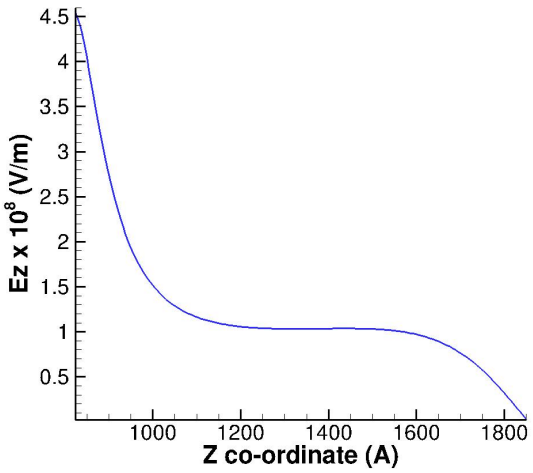

(c) Linear variation of the normal electric field along $y = 0$.

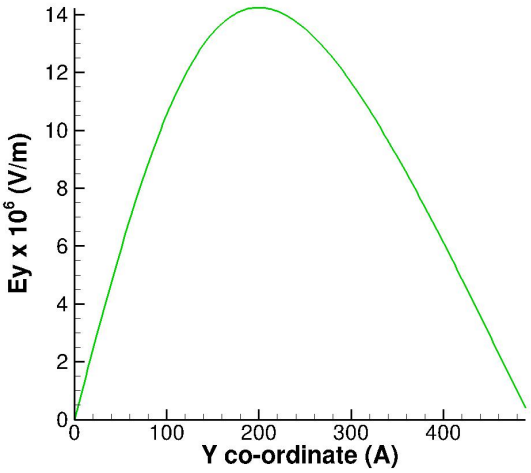

(d) Linear variation of the radial electric field along $z = 1,000$.

Figure 2. The electric fields generated by solving Eq. 1 with the boundary conditions shown in Fig. 1(a) and extraction voltage of -17 V.

term represents the potential due to the external electric fields. Equation 1 was solved using the generalized minimal residual (GMRES) method[48] with a grid-size (h_x, h_y, and h_z) equal to the Coulomb cut-off radii, $R_c = 20$ Å. Note that the contribution from the second term of Eq. 2 to the total electric potential on a CG site only needs to be computed once, at the zero-th time step, whereas, the first term of Eq. 2 was computed every time step in the MD simulation. Grid convergence for Eq. 1 was tested by reducing the grid size from 20 to 5.0 Å.

It was observed that the solution to Eq. 1, using the boundary set-up and conditions shown in Fig. 1(a) and an extraction voltage of -17 V generated an external electric field with normal as well as radial components, as shown in Figs. 2(a) and 2(b), respectively. Both,

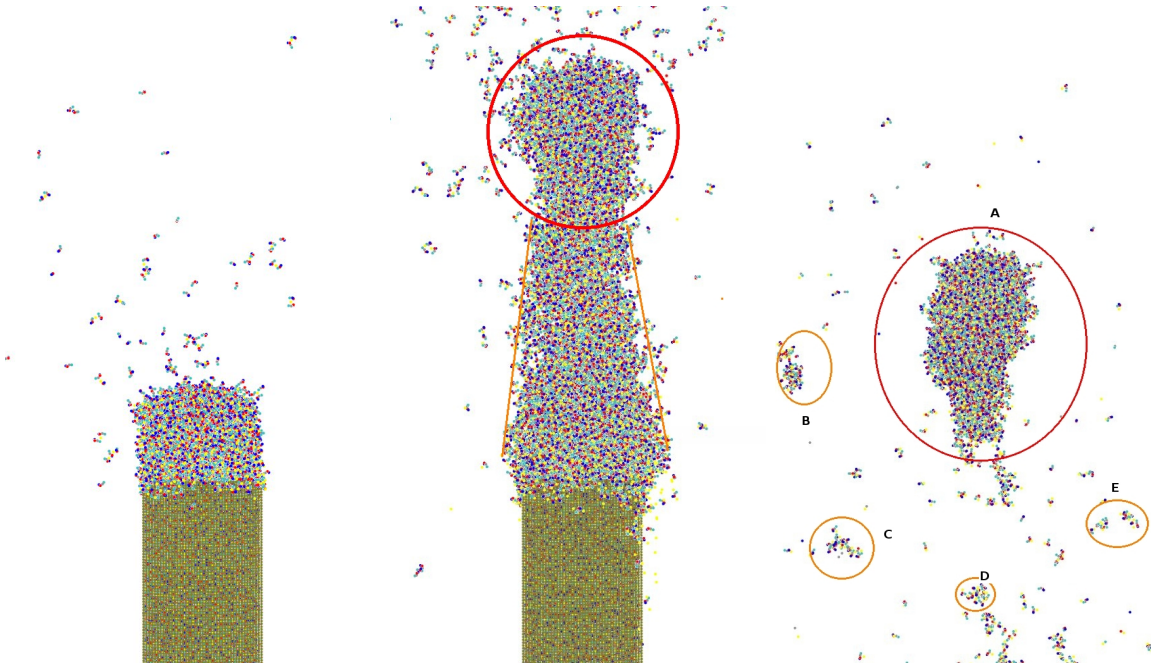

(a) At t = 700 ps. (b) At t = 800 ps. (c) At t = 950 ps.

Figure 3. Snapshot of electrospray and droplet formation from coarse-grained MD simulation of EMIM-BF_4. Mass flow rate and extraction potential of 1.09×10^{-11} kg/s and -17 V, respectively. Atom colors are: M1 (teal), IM (silver), MR (red), M2 (navy), BF_4 (yellow), and Pt (bronze). The capillary diameter is 112 Å and vertical dimensions are 800 Å.

the normal and radial electric field components are strongest at the meniscus or mouth of the capillary and become gradually weaker away from the mouth of the capillary. It was found that the presence of the radial electric field near the capillary meniscus is necessary to generate the Taylor cone shape.[30] The unique shape of the electric field also effects the stability of the Taylor cone and the type of ions species that are emitted from it.

The variation in the normal and radial electric fields can be better viewed by extracting the values along the gray center-line in Fig. 2(a). Along the center-line of the capillary, the normal electric field is highest at the mouth of the capillary and decreases rapidly within 300 Å from the mouth of the capillary or z = 1,125 Å, as shown in Fig. 2(c). The normal electric field remains constant throughout rest of domain but starts decreasing close to the extractor plane, located at z = 1,825 Å. The radial electric field variation along the tangential direction was obtained by extracting values along the z = 1,000 Å, shown in Fig. 2(b). The radial electric field is zero at the center-line or axis of the capillary and near the boundaries, as shown in Fig. 2(d).

III. Role of normal and radial electric fields on the MD simulations

A. Formation of the Taylor cone and emission characteristics

The snapshot of the formation of the Taylor cone from the MD simulations are shown in Fig. 3. The high mass flow rate through the capillary does not allow instantaneous formation

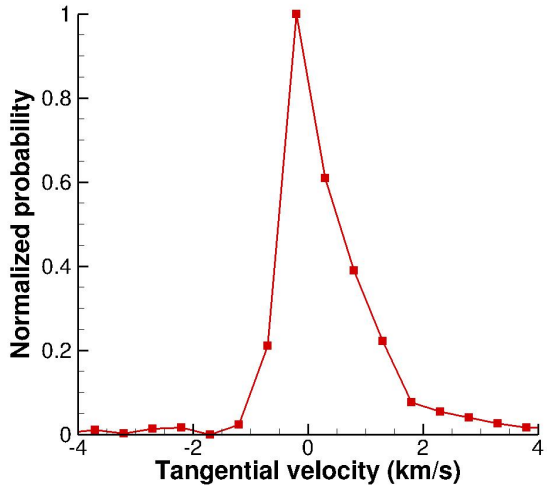

(a) Tangential (V_x and V_y) velocities of droplets.

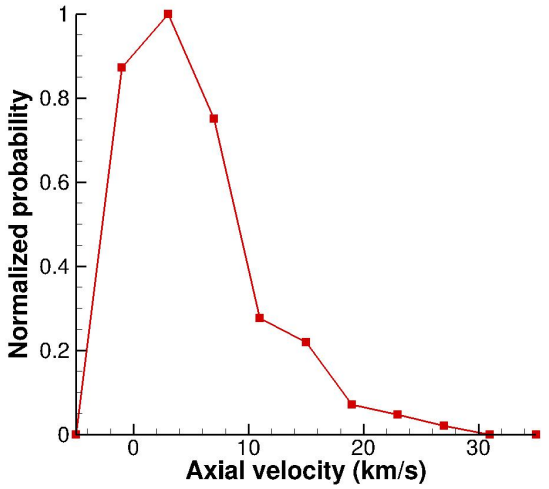

(b) Axial (V_z, towards the extractor plane) velocities of droplets.

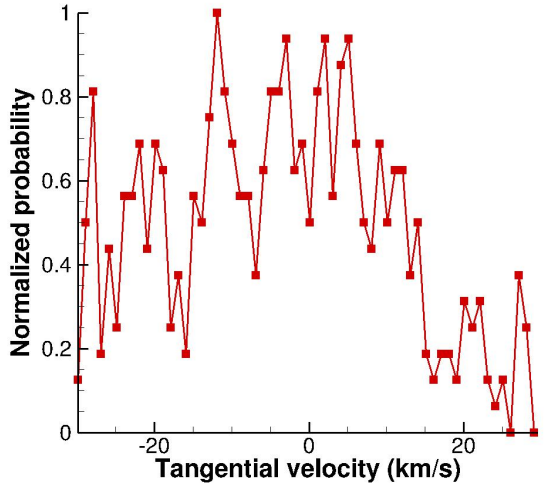

(c) Tangential (V_x and V_y) velocities of monomers.

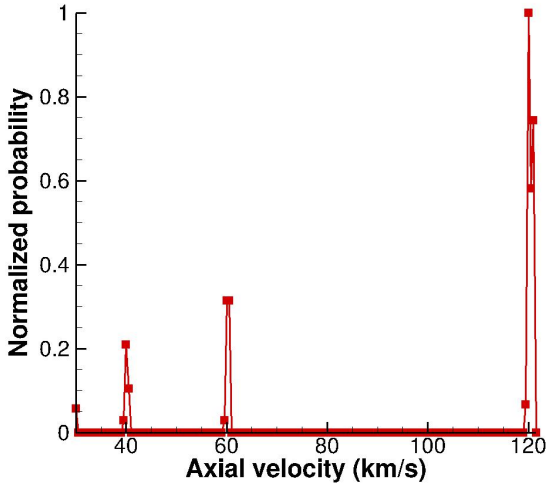

(d) Axial (V_z, towards the extractor plane) velocities of monomers.

Figure 4. The tangential and axial velocity distributions of the monomers and droplets emitted from an EMIM-BF_4 electrospray. Total number of droplets and monomers sampled are 390 and 321, respectively.

of the Taylor cone and the ion-pairs flow out of the capillary with a contiguous cylindrical shape, at 600 ps simulation time, as shown in Fig. 3(a). At 700 ps, the combination of the normal and radial electric field start shaping the emitted mass into a cone shaped structure, as shown in Fig. 3(b). This constriction results in a large IL droplet, consisting of 2,614 EMIM-BF_4 ILs to form at the tip of the cone structure. As shown in Fig. 3(c), after 800 ps, this primary droplet, titled 'A', is isolated away from the tip of the Taylor cone structure as it travels towards the extractor plane along with other aggregates (see 'B - E'). The Taylor cone apex is formed approximately 200 Å above the mouth of the capillary, i.e., at

z = 1,025 Å from the base of the capillary. The details of Taylor cone formation and the sampled ion species has been published in our previous work.[30,46]

It is relevant to analyze the differences in the emission of smaller ion species versus the larger droplets, as it allows for a better understanding of the Taylor cone formation. We hypothesized that EMIM-BF_4 ion-pairs are either emitted as monomers from the sides of the Taylor cone or as larger ion-species from the tip of the Taylor cone. This was verified by generating velocity distributions of the monomers and droplets. A sampling plane located at 100 Å above the Taylor cone (z = 1,125 Å) was selected because at that location the emitted droplets and monomers do not undergo further acceleration and maintain their emitted velocities. This location also ensures that we obtain sufficient droplet statistics, since the droplets break down into smaller emission species as they travel towards the extractor plane. The tangential and axial velocity distributions of the droplets are shown in Figs. 4(a) and 4(b). Tangential velocities are generated because of the interaction of radial electric field with the emitted ion species. The shape of the tangential velocity distribution of droplets has the form of a normal distribution with a mean value close to zero, suggesting that the majority of droplets emitted from the capillary have negligible tangential velocities. Since the radial electric fields are weakest near the tip of the capillary, we can interpret Fig. 4(a) to show that the droplets lack tangential velocities because they are emitted from the tip of the Taylor cone. The distribution of droplet axial velocities, shown in Fig. 4(b), suggests that majority of the droplet are emitted with an axial velocity between 5 and 10 km/s. In contrast, a similar analysis of monomer velocities does not give this result. The monomer tangential velocity distribution, shown in Fig. 4(c), does not have a maximum probability close to zero, but instead exhibits a noticeable number of samples at non-zero tangential velocities. This result suggests that emitted monomers interact with the radial electric field and since the field is strongest near the sides of the Taylor cone, we can conclude that majority of the monomers are emitted from the sides of the Taylor cone, as was concluded by Lozano[49] for his experimental studies on the EMIM-BF_4 electrosprays. Finally, because the mass of monomers is comparatively much lower than that of droplets, they are strongly accelerated in the axial direction with no clear maxima, as shown in Fig. 4(d).

B. Evolution of the primary droplet in the applied electric field

As noted previously, during the extrusion simulation, the emitted ion-species travel towards the extractor plane, which is only 1,000 Å away from the mouth of the capillary but these ion-species travel on the order of micro-meters during experimental electrospray operations. The larger aggregate may break down into smaller species as they travel longer distance towards the extractor plane in the presence of an external electric field. To replicate this process, we isolate the large droplet emitted from the extrusion simulation, shown as group 'A' in Fig. 3(c). This droplet is at least 40 Å away from either the Taylor cone or any other aggregate and therefore does not have Coulomb interaction contributions from other ion-pairs in the domain. To study further break-up of this large droplet, the primary droplet was simulated in a quasi-infinite domain for a range of normal and radial electric fields typically experienced by the droplet during its motion from the tip of the capillary to the extractor plane. For the extraction voltage of -17 V and the simulation domain shown in Fig. 1(a), the region between the tip of the Taylor cone and the extractor plane (between z = 1,125 Å and z = 1,825 Å) has a normal electric field range between 0.05 - 0.15 V/nm.

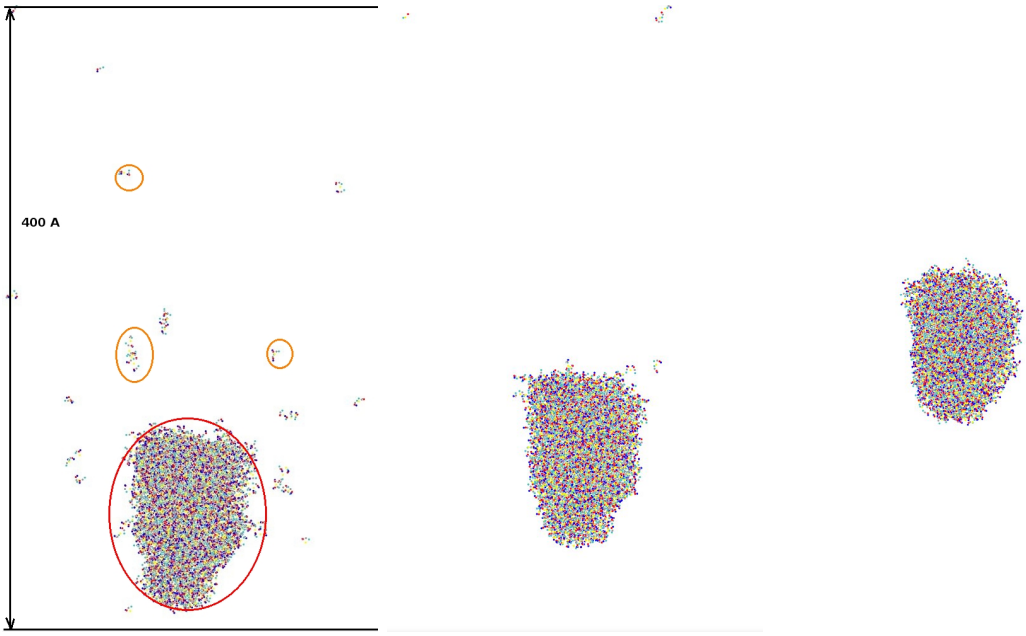

(a) At $t = 100$ ps. (b) At $t = 200$ ps. (c) At $t = 300$ ps.

Figure 5. Snapshot of isolated droplet simulations using coarse-grained EMIM-BF_4. Normal and radial electric fields are 0.05 V/nm and 0.005 V/nm, respectively. Atom colors are: M1 (teal), IM (silver), MR (red), M2 (navy), BF_4 (yellow), and Pt (bronze). The droplet diameter is 100 Å and vertical dimensions are 400 Å.

As established previously, the large droplets are emitted from the tip of the Taylor cone, along the axis of the capillary, where the radial electric fields are weakest. Therefore, we can assume that the droplet will experience radial electric fields in the range 0.001 - 0.01 V/nm.

Multiple MD simulations of the primary droplet were performed for the discussed range of the normal and radial electric fields. Snapshots of the primary droplet simulation for a normal and radial electric field strength of 0.05 V/nm and 0.005 V/nm are shown in Fig. 5. The time for the primary droplet simulations shown in Fig. 5 represents simulation time beyond the initial 950 ps required for the droplet to form during the extrusion simulation. It was observed that several ion-species (monomer, dimer, and trimer) and droplets were emitted during the first 100 ps (total time 100 + 950 = 1,050 ps) of the simulations, as shown in Fig. 5(a). The smaller species and droplets (circled in orange) emitted from the larger primary droplet (circled in red) are accelerated by the electric field and travel faster than the large droplet. After 200 ps, the smaller ion aggregates move 300 Å away from the larger droplet, as shown in Fig. 5(b) and the rate of emission of the smaller ion species emitted from the larger droplet reduces substantially. The smaller aggregates emitted from the larger droplet travel faster than the droplet due to their lower mass. The emission of smaller ion aggregates from the larger droplet stops completely after 300 ps, as shown in Fig. 5(c). The rate of emission of smaller species from the droplet is strongly dependent on the external electric fields, as discussed in the following sub-section.

The ion aggregates emitted from the primary droplet were counted 400 Å above the instantaneous center-of-mass of the larger droplet. Ion aggregates were counted during the entire period of the simulation up to the time when the primary droplet stopped emitted any more ion aggregates. In Fig. 6(a), the total number of emitted ion aggregates are shown

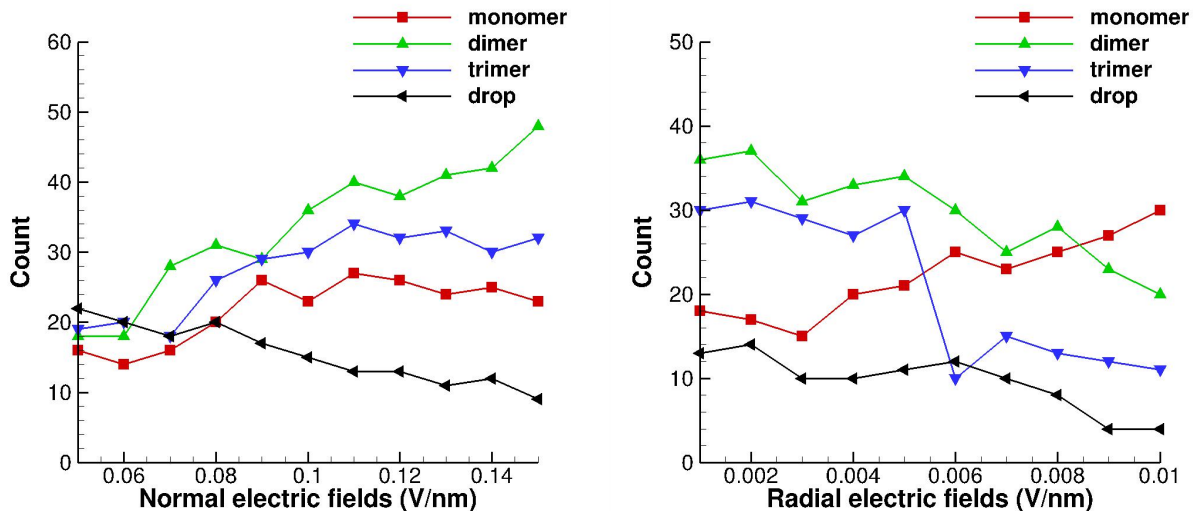

(a) Effect of normal electric field, using constant radial electric field of 0.005 V/nm.

(b) Effect of radial electric field, using constant normal electric field of 0.10 V/nm.

Figure 6. Emitted ion-species as a function of normal and radial electric fields.

as a function of normal electric field. It was observed that at the lowest normal electric fields, the emission of smaller droplet from the primary droplet was maximum followed by trimers, dimers, and monomers. As the normal electric field was increased, the smaller ion-aggregates, such as dimers, trimers, and monomers were the dominant emitted species. The higher magnitude of normal electric field weakens the electrostatic forces required to form smaller droplets from the primary droplet, resulting in higher emission of smaller ion species.

Similarly, the number of small droplets emitted from the larger primary droplet decreased as the radial electric field was increased, as shown in Fig. 6(b). Concurrently, even the number of emitted dimers and trimers decreased when the radial electric field was increased. In contrast, the radial electric field enhanced the emission of monomers from the primary droplet. The primary droplet used for the simulation is not a perfect sphere but a prolate geometry. Thus, the radial electric field acts on a larger surface area on the sides of the prolate droplet, allowing for easier emission of smaller monomers rather than larger droplets from the top of the droplet.

C. Effect of electric fields on the final droplet mass and volume

The volume and total mass of the primary droplet were tracked during the isolated droplet simulation as a function of time. Figure 7 shows the decrease in droplet volume and mass for different applied normal electric fields. As previously stated, the simulation time shown in Fig. 7 is beyond the 950 ps required to emit and isolate the droplet from the capillary. The results shown in Fig. 7 were obtained for the radial electric field of 0.005 V/nm. For the simulations performed with a normal electric field of 0.05 V/nm, the initial emission of smaller ions and the resulting initial decrease in the droplet volume occurred during the initial 200 ps of the simulation, as shown in Fig. 7(a). When the normal electric field was increased to 0.1 V/nm, this rapid decrease in the volume occurs in approximately 100 ps, as shown in Fig. 7(b), and reduces to 50 ps for the highest normal electric field of 0.15 V/nm.

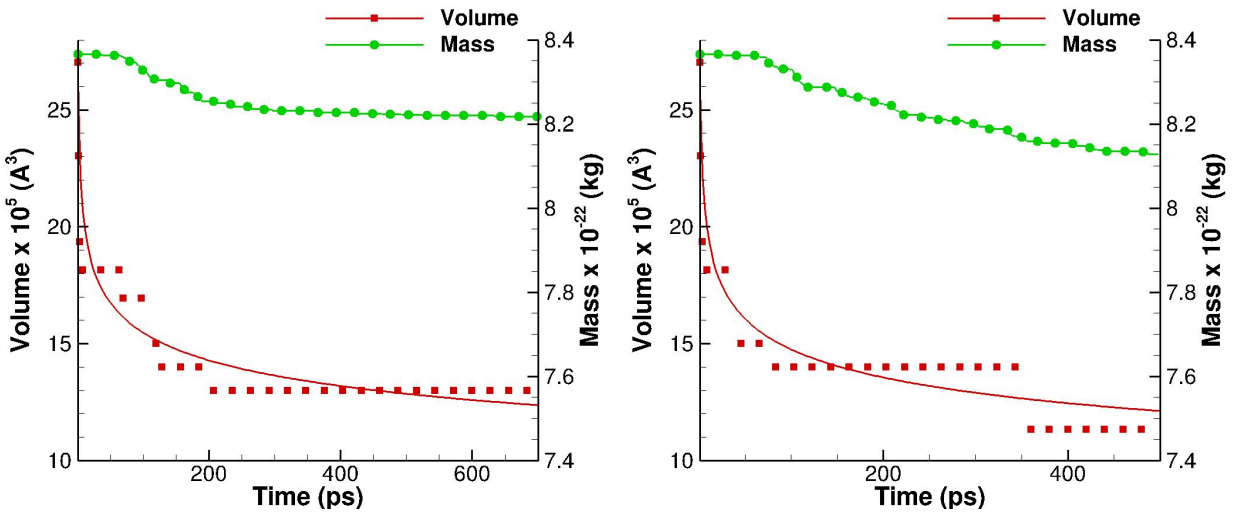

(a) Normal electric field strength 0.05 V/nm.

(b) Normal electric field strength 0.10 V/nm.

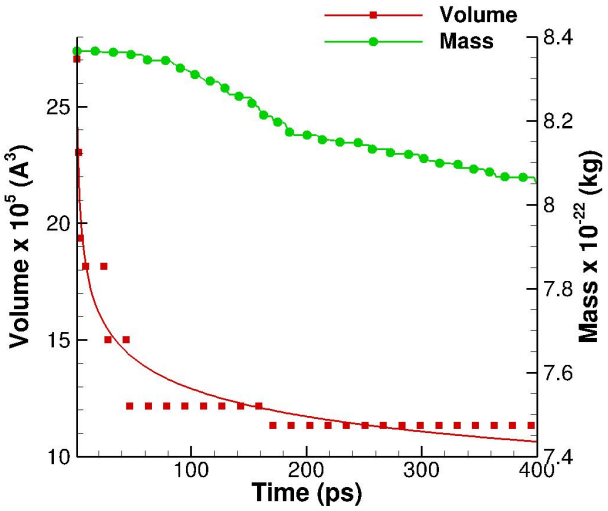

(c) Normal electric field strength 0.15 V/nm.

Figure 7. Droplet volume and total mass as a function of simulation time for the radial electric field of 0.005 V/nm. The normal electric field strengths are provided in the figure captions.

The volume and mass of the droplet did not show significant change after the initial rapid emission of ion aggregates from the droplet, even when the simulations were allowed to run for extended time of 1,200 ps.

The final mass and volume of the droplet was found to depend on the strength of the electric fields. The effect of normal and radial electric field on the final droplet mass is shown in Figs. 8(a) and 8(b), respectively. A least square fit of the data points shows a linear relationship between the normal and radial electric fields and the final droplet mass, such that the slopes of the least square fit are negative. Not surprisingly, the final droplet mass decreased if either the normal or radial electric fields were increased. From the negative slopes of the least square fit, we can infer that increasing the radial electric fields will produce droplets with lower final mass compared to that by increasing the normal electric field. Due

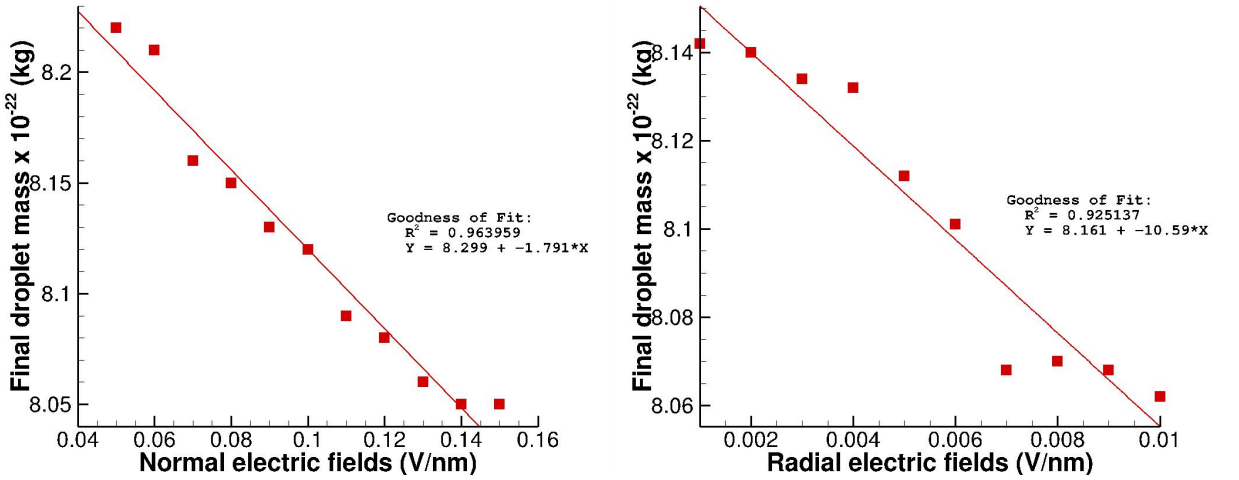

(a) Effect of normal electric field, using constant radial electric field of 0.005 V/nm.

(b) Effect of radial electric field, using constant normal electric field of 0.10 V/nm.

Figure 8. Final droplet mass as a function of normal and radial electric fields.

to the irregular shape of the droplet (not a perfect sphere) and its orientation during the primary droplet simulations, the radial electric fields were found to be more effective but not necessarily faster at removing mass from the droplet.

The normal and radial electric fields also influence the rate of volume decay of the main droplet. From our analysis of the primary droplet simulations, it was observed that a power law would be the best mathematical representation of the change in the volume of the droplet. So, power law equation was used to generate a curve fit for the volume loss of the droplet as a function of the simulation time, as shown in Fig. 7. The equation used for curve-fitting has the following form,

$$y = e^{p*ln(x)+c} \tag{3}$$

where, c is the initial droplet volume, x is the simulation time, and p is the decay rate of the droplet volume. The decay rate for all primary droplet simulations were calculated and analyzed as a function of the normal or radial electric fields used for the primary droplet simulations. A least square fit of the obtained volume decay rates was generated for both the normal and radial electric field cases, as shown in Figs. 9(a) and 9(b), respectively. From the slope of the least square fit, we can state that the decay rate, p, has a linear dependence on the normal electric field, shown in Fig. 9(a), suggesting that the droplet would lose mass and its corresponding volume faster if the magnitude of the normal electric field was increased. Although, a similar analysis also shows the linear dependence of decay rate with the magnitude of the radial electric fields, shown in Fig. 11(b), this result does not provide a true representation of the droplet volume decay in the radial electric fields. The slope of the least square fit is positive suggesting that the droplet decay rate reduces when the magnitude of the radial electric field was increased, which is counter-intuitive but valid. From our simulations, we observed that when the droplet was placed in a strong radial electric field, the initial loss of smaller aggregates from the droplet was not symmetric. This created an imbalance in the distribution of charges within the droplet, which generated a biased

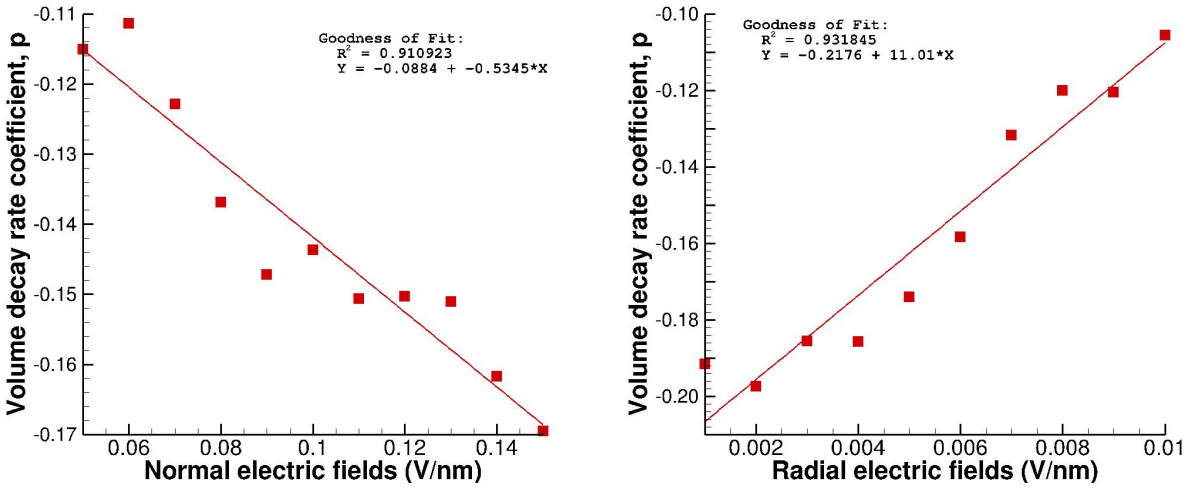

(a) Effect of normal electric field, using constant radial electric field of 0.005 V/nm.

(b) Effect of radial electric field, using constant normal electric field of 0.10 V/nm.

Figure 9. Volume decay rate as a function of normal and radial electric fields.

movement of the entire droplet towards one of the four quadrants shown in Fig. 1(b). Since the droplet no longer experiences symmetric radial fields, the radial electric fields become ineffective in removing further mass from the droplet, leading to a reduction in the volume decay rate. However, it should be noted that this result is not in conflict with that shown in Fig. 8(b) because, the maximum mass loss of the droplet occurs during initial time-steps, when the droplet experiences symmetric radial fields, and not during the later time steps when the droplet is entirely within one of the four quadrants.

D. Comparison of MD results with Rayleigh instability and Coulomb fission models

The charge residue method (CRM)[42,50] and the ion evaporation mechanism (IEM)[44] are the two notable experimentally suggested theories traditionally used to study of the disintegration of the large droplets emitted by the electrosprays.[38] The CRM proposes that the smaller ions from the larger droplets are generated by successive instabilities in the larger droplet, as described by the Rayleigh[43] theory. According to Rayleigh, the number of charges required for the instabilities to exist in the droplet, also known as the Rayleigh limit depends on the physical and electrochemical properties of the droplet. The Rayleigh limit for the droplet can be calculated using Eq. 4,[39]

$$z^2 = 64\pi^2\epsilon_0\gamma r^3/e^2 \tag{4}$$

where, z is the number of charges, $\epsilon_0 = 8.8541 \times 10^{-12}$ F/m is the permittivity of vacuum, γ is the surface tension, $e = 1.60217 \times 10^{-19}$ C is the elementary charge, and r is the radius of the droplet. The EMIM-BF_4 has a surface tension of $\gamma = 52$ dyn/cm[51] and the approximate radius of the EMIM-BF_4 primary droplet was calculated using the mass density, $\rho = 1,260$ kg/m^3 and an initial droplet mass of 8.365×10^{-22} kg. The approximate radius of the droplet was $r = 54$ Å and the critical charges required for Rayleigh instabilities calculated using Eq. 4 was $z = 43$. The initial charge of the primary droplet used for the MD simulation, $z = 158$

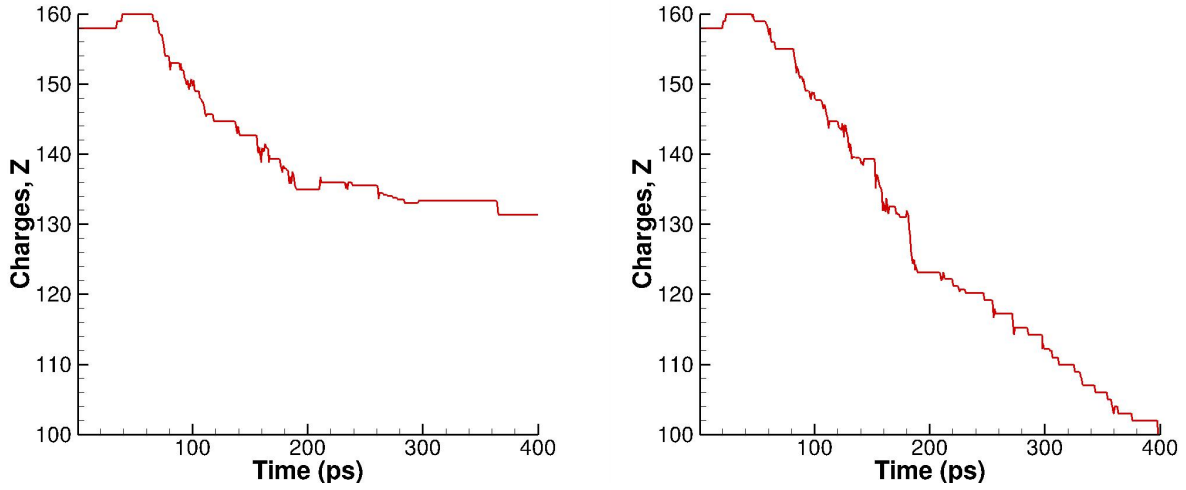

(a) Normal electric field of 0.05 V/nm.

(b) Normal electric field of 0.15 V/nm.

Figure 10. Final droplet charge as a function of normal and radial electric fields.

is much higher than that critical threshold of $z = 43$, suggesting that the primary droplet will definitely undergo further disintegration. During the MD simulations, we monitored the total number of charges as a function of time, as shown in Fig. 10(a) and 10(b). However, it should be noted that even for the highest normal electric fields, the final total charge of the droplet was still higher than the critical Rayleigh limit but the droplet did not undergo further disintegration. It is also possible to calculate the electric field normal to the surface, E_s associated with the electrostatic forces of a charged droplet necessary using Eq. 5,[33]

$$E_s = \frac{ze}{4\pi\epsilon_0 r^2} \tag{5}$$

such that the total electric field to completely overcome the electrostatic forces of a droplet with $z = 158$ and $r = 54$ Å is $E_s = 7.77$ V/nm. For the given Rayleigh limit, using Eq. 5, we can also estimate the electric field required to generate the Rayleigh instabilities in the droplet.

$$E_{R_y} = \left(\frac{4\gamma}{\epsilon_0 r}\right)^{1/2} \tag{6}$$

Using Eq. 6, the required electric field for Rayleigh disintegration was $E_{R_y} = 2.083$ V/nm. Both, the electric fields associated with the droplet charge and the field required for Rayleigh disintegration are much higher than the highest normal and radial electric fields used for the simulations. This could explain why the droplet does not undergo further disintegration during the simulations even when the simulation time is extended to 1,200 ps.

We also used the Born model, which is a basic component of the IEM, to calculate the predicted radius of the ion species emitted from the large droplet, using Eq. 7.[38]

$$R_B = \left(\frac{e^2}{64\pi^2\epsilon_0\gamma}\right)^{1/3} \tag{7}$$

The Born radius for EMIM-BF_4 is $R_B = 4.45$ Å, which is the approximate radius of the dimer. As shown in Figs. 6(a) and 6(b), the dimers were the dominant emitted species during the

MD simulations, suggesting that our simulations are in agreement with the theoretically obtained values. However, the Born model does not provide any information regarding the emission of smaller droplets from the original droplet. We therefore use the Coulomb fission model to obtain the theoretical prediction of the secondary droplet radius, R_s.[52]

$$R_s = \left(\frac{3\pi}{2^8}\right)^{1/3} r \tag{8}$$

Using the Coulomb fission model, we get a secondary droplet radius, $R_s = 16.68$ Å, which is approximately equal to the radius of the secondary droplets, consisting of 9 or more cations and 8 anions, emitted during our primary droplet MD simulations.

The Coulomb fission model also allows one to calculate the jet break-up time as an inverse of the jet growth rate, α_m.

$$t_{break} = \frac{1}{\alpha_m} \tag{9}$$

The jet growth rate is related to the physical and electro-chemical properties of the IL. Equation 10 is used for calculating α_m.

$$\alpha_m = \left(\frac{4\sigma^6}{27\epsilon^3\gamma^2\rho}\right)^{1/2} \tag{10}$$

where, $\epsilon = 15$[53] is the dielectric permittivity of EMIM-BF_4 and σ, the surface charge density is calculated using Eq. 11.

$$\sigma = \left(\frac{27\epsilon^3\gamma^2\rho I}{4\pi^2 r^4}\right)^{1/8} \tag{11}$$

The surface current, I, is calculated using Eq. 12,

$$I = \left(\frac{3\pi^6\epsilon\gamma^2}{2^6\rho}\right)^{1/2}. \tag{12}$$

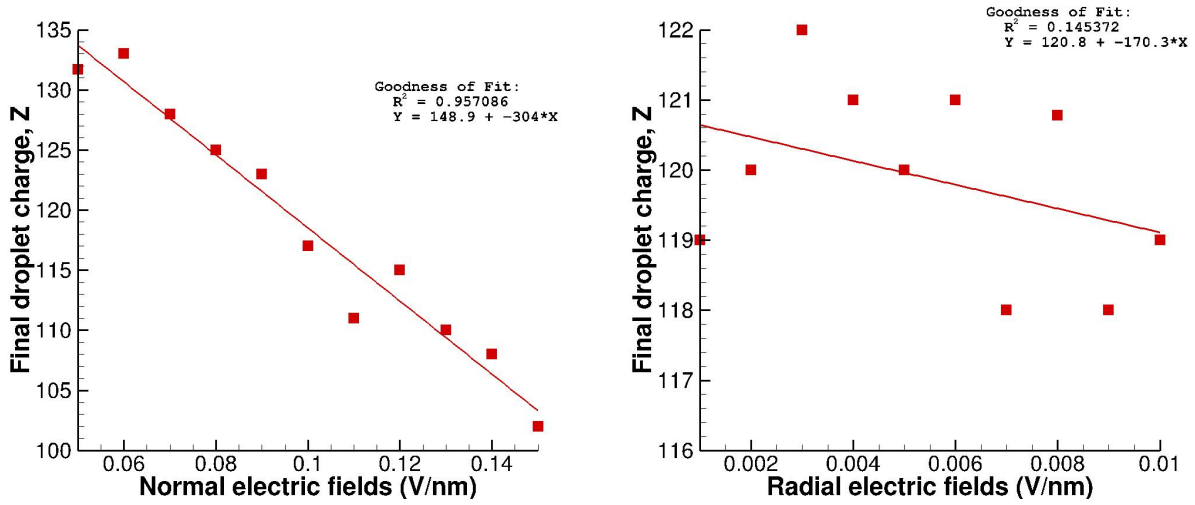

(a) Effect of normal electric field, using constant radial electric field of 0.005 V/nm.

(b) Effect of radial electric field, using constant normal electric field of 0.10 V/nm.

Figure 11. Final droplet charge as a function of normal and radial electric fields.

For the EMIM-BF_4 droplet of radius, $r = 54$ Å, using Eqs. 9 - 12, the jet breakdown time was $t_{break} = 44$ ps. In Figs. 10(a) and 10(b), each decrease or rise in the total droplet charge represents the emission of a secondary ion-species or droplet. The larger decline signify the emission of larger aggregate from the original droplet and the smaller drops represent the emission of monomers, dimers, and trimers. From Fig. 10(a), sharp decrease in the droplet charge at $t = 50$, 175, and 225 occur after 30-40 ps of no change in the droplet charge, thus providing a reasonable agreement between the simulations and the jet breakdown time predicted by the Coulomb emission theory. As expected, for higher electric field strengths and as the original droplets gets smaller due to mass loss, the emission time reduces to approximately 20 ps, as shown in Fig. 10(b).

The final droplet charges also depend on the strength of the normal and radial electric fields. A linear dependence of the final droplet charge on the normal electric field is obtained, as shown in Fig. 11(a). The charge-to-mass (z/m) ratio of monomers, dimers, and trimers is higher than that of the secondary smaller droplets emitted by the original droplet. At higher normal electric fields, the original droplets emits more dimers, monomers, and trimers and less secondary droplets, resulting in higher loss of charge from the original droplet. In contrast, no dependency was observed between the final droplet charges and the radial electric field strengths, as shown in Fig. 11(b). This may be due to the irregular shape of the droplet used for the simulation as well as conservative range of radial electric field values used for the simulations.

IV. Conclusion

The MD simulations of an primary EMIM-BF_4 droplet provided key insight regarding the evolution and final state of large droplets emitted during an electrospray process. The results obtained from this work can be used as initial conditions for larger length-scale models, such as, the kinetic Monte Carlo methods. Conventional theories, such as, CRM and IEM predict a complete disintegration of large droplets into gaseous ion species but from MD simulations, we observed that large droplet does not undergo disintegration after certain mass is reached. A dependence of droplet mass and volume on the strengths of the normal and radial electric fields was also observed. In the presence of strong radial electric fields, an unsymmetrical loss of mass was observed, which resulted in the lateral motion of the droplet. The faster loss of charges during the initial time steps and the subsequent lateral motion of the droplet reduced the rate of volume decay.

A good agreement was obtained between the theoretically predicted Born radius and the secondary emission species emitted during the simulations. The radius of the secondary droplets emitted during the simulations compared well the radius predicted by the Coulomb fission theory. The time between the emission of secondary droplet was found to be comparable to the jet breakdown time obtained from the Coulomb fission model. While the final droplet charges were found to be in linear dependence with the normal electric fields, no such correlation was obtained between the charges and the radial electric field strengths.

Moving forward, further analysis will be performed to understand the non-symmetrical mass loss of the droplet when the radial electric fields are increased. The normal electric field range will also be increased closer to the field values required for Rayleigh disintegration of the droplet. This will allow us to address questions that may not be adequately answered

by the theoretical models, especially, the dependence of secondary droplet sizes and the dominant emission species on the applied external electric fields. The methods and tools used for the simulations of the EMIM-BF_4 droplet can be easily extended to perform similar simulations of other IL droplets.

Acknowledgments

Funding for this work was provided by the Air Force Office of Scientific Research (AFOSR) through Dr. Mittat Birkan under Grant No. AF FA9550-16-1-0193. We are thankful to the Department of Defense for providing us with the vital computational resources on their GARNET and to and XSEDE TACC for their use of STAMPEDE2 cluster.

References

References

[1]Lebourgeois, V., Dupuy, S., Vintrou, E., Ameline, M., Butler, S., and Bgu, A., "A Combined Random Forest and OBIA Classification Scheme for Mapping Smallholder Agriculture at Different Nomenclature Levels Using Multisource Data (Simulated Sentinel-2 Time Series, VHRS and DEM)," *Remote Sensing*, Vol. 9, No. 3, March 2017.

[2]Tsitas, S. R. and Kingston, J., "6U CubeSat commercial applications," *The Aeronautical Journal*, Vol. 116, No. 1176, February 2012, pp. 189198.

[3]Krebs, M., "Satellite Constellation," March 2016, US Patent App. 14/501,859.

[4]M., G. D. and Katz, I., *Fundamentals of Electric Propulsion: Ion and Hall Thrusters*, John Wiley and Sons, 2008.

[5]Mitterauer, J., "Field Emission Electric Propulsion: Emission Site Distribution of Slit Emitters," *IEEE Transactions on Plasma Science*, Vol. 15, No. 5, October 1987, pp. 593–598.

[6]Taylor, G. I., "Disintegration of Water Droplets in an Electric Field," *Proceedings of Royal Society A*, Vol. 280, No. 1328, 1964, pp. 383–397.

[7]Deng, W., Waits, C. M., and Gomez, A., "Digital electrospray for controlled deposition," *Review of Scientific Instruments*, Vol. 81, No. 3, March 2010, pp. 035114.

[8]Jaworek, A., "Electrospray droplet sources for thin film deposition," *Journal of Materials Science*, Vol. 42, No. 1, January 2007, pp. 266–297.

[9]Swanson, L., "Liquid metal ion sources: Mechanism and applications," *Nuclear Instruments and Methods in Physics Research*, Vol. 218, No. 1, December 1983, pp. 347–353.

[10]Clampitt, R., "Advances in molten metal field ion sources," *Nuclear Instruments and Methods in Physics Research*, Vol. 189, No. 1, October 1981, pp. 111–116.

[11]Wu, Y., Kennedy, S. J., and Clark, R. L., "Polymeric particle formation through electrospraying at low atmospheric pressure," *Journal of Biomedical Materials Research Part B: Applied Biomaterials*, Vol. 90B, No. 1, 2009, pp. 381–387.

[12]Zhu, W., Castro, N. J., Cheng, X., Keidar, M., and Zhang, L. G., "Cold Atmospheric Plasma Modified Electrospun Scaffolds with Embedded Microspheres for Improved Cartilage Regeneration," *PLoS ONE*, Vol. 10, No. 7, 07 2015, pp. e0134729.

[13]Wu, B. and Becker, J. S., "Imaging of elements and molecules in biological tissues and cells in the low-micrometer and nanometer range," *International Journal of Mass Spectrometry*, Vol. 307, No. 1, October 2011, pp. 112–122.

[14]Jayasinghe, S. N. and Sullivan, A. C., "Electrospraying: an in-situ polymerisation route for fabricating high macroporous scaffolds," *Journal of Sol-Gel Science and Technology*, Vol. 38, No. 3, 2006, pp. 293–302.

[15]Jayasinghe, S. N., Qureshi, A. N., and Eagles, P. A. M., "Electrohydrodynamic Jet Processing: An Advanced Electric-Field-Driven Jetting Phenomenon for Processing Living Cells," *Small*, Vol. 2, No. 2, 2006, pp. 216–219.

[16]Toniolo, R., Pizzariello, A., Dossi, N., Lorenzon, S., Abollino, O., and Bontempelli, G., "Room Temperature Ionic Liquids As Useful Overlayers for Estimating Food Quality from Their Odor Analysis by Quartz Crystal Microbalance Measurements," *Analytical Chemistry*, Vol. 85, No. 15, 2013, pp. 7241–7247.

[17]"The effect of processing variables on the morphology of electrospun nanofibers and textiles," *Polymer*, Vol. 42, No. 1, 2001, pp. 261 – 272.

[18]Jirsak, J., Moucka, F., and Nezbeda, I., "Insight into Electrospinning via Molecular Simulations," *Industrial & Engineering Chemistry Research*, Vol. 53, No. 19, 2014, pp. 8257–8264.

[19]Jahn, R. G. and Choueiri, E. Y., *Encyclopedia of Physical Science and Technology, Electric Propulsion*, Vol. 5, Academic Press, 3rd ed., 2002.

[20]Gamero-Castano, M. and Hruby, V., "Electrospray as a source of Nanoparticles for Efficient Colloid Thrusters," *Journal of Propulsion and Power*, Vol. 17, No. 5, October 2001, pp. 977–987.

[21]Hruby, V., Gamero-Castano, M., Spence, D., Gasdaska, C., Demmons, N., McCormick, R., Falkos, P., Young, J., and Connolly, W., "Colloid thrusters for the new millennium, ST7 DRS mission," *2004 IEEE Aerospace Conference Proceedings (IEEE Cat. No.04TH8720)*, Vol. 1, March 2004, p. 213 Vol.1.

[22]Donius, B. and Rovey, J. L., "Ionic Liquid Dual-Mode Spacecraft Propulsion Assessment," *Journal of Spacecraft and Rockets*, Vol. 48, No. 1, 2011, pp. 110–123.

[23]Prince, B. D., Tiruppathi, P., Bemish, R. J., Chiu, Y.-H., and Maginn, E. J., "Molecular Dynamics Simulations of 1-Ethyl-3-methylimidazolium Bis[(trifluoromethyl)sulfonyl]imide Clusters and Nanodrops," *The Journal of Physical Chemistry A*, Vol. 119, No. 2, 2015, pp. 352–368.

[24]P., A. M. and Tildesley, D. J., *Computer Simulations of Liquids*, Oxford Science Publications, 2009.

[25]Borner, A. and Levin, D. A., *Use of advanced particle methods in modeling space propulsion and its supersonic expansions*, PHD Dissertations, PSU, 2014.

[26]Wang, Y., Noid, W., and Voth, G., "Effective Field Coarse Graining," *Physical Chemistry Chemical Physics*, Vol. 11, 2009, pp. 2002–2015.

[27]Wang, Y., Izvekov, S., Yan, T., and Voth, G., "Multiscale coarse-graining of Ionic Liquids," *Journal of Physical Chemistry B*, Vol. 110, 2005, pp. 3564–3575.

[28]Noid, W., Chu, J.-W., Ayton, G., Krishna, V., Izvekov, S., Voth, G., Das, A., and H.C., A., "The multiscale coarse-graining method I. A rigorous bridge between atomistic and coarse-grained models," *The Journal of Chemical Physics*, Vol. 128, 2008, pp. 244114.

[29]Romero-Sanz, I., Bocanegra, R., Fernandez de la Mora, J., and Gamero-Castano, M., "Source of heavy molecular ions based on Taylor cones of ionic liquids operating in the pure ion evaporation regime," *Journal of Applied Physics*, Vol. 94, No. 5, June 2003, pp. 3599–3605.

[30]Mehta, N. A. and Levin, D. A., "Effects of Long-range Coulomb interaction models on the Electrospray Molecular Dynamics Simulations," *Physical Review E*, under review.

[31]Borner, A., Wang, P., and Levin, D. A., "Influence of electrical boundary conditions on molecular dynamics simulations of ionic liquid electrosprays," *Physical Review E*, Vol. 90, Dec 2014, pp. 063303.

[32]Borner, A., Li, Z., and Levin, D., "Prediction of Fundamental Properties of Ionic Liquid Electrospray Thrusters using Molecular Dynamics." *Journal of Physical Chemistry B*, Vol. 117, No. 22, 2013, pp. 6768–6781.

[33]Kebarle, P. and Peschke, M., "On the mechanisms by which the charged droplets produced by electrospray lead to gas phase ions," *Analytica Chimica Acta*, Vol. 406, No. 1, February 2000, pp. 11 – 35.

[34]Konermann, L., "A Simple Model for the Disintegration of Highly Charged Solvent Droplets during Electrospray Ionization," *Journal of the American Society for Mass Spectrometry*, Vol. 20, No. 3, November 2009, pp. 496 – 506.

[35]Gomez, A. and Tang, K., "Charge and fission of droplets in electrostatic sprays," *Physics of Fluids*, Vol. 6, No. 1, 1994, pp. 404–414.

[36]Duft, D., Achtzehn, T., Muller, R., Huber, B. A., and Leisner, T., "Coulomb fission: Rayleigh jets from levitated microdroplets," *Nature*, Vol. 421, No. 128, January 2003, pp. 1.

[37]Li, D., Marquez, M., and Xia, Y., "Capturing electrified nanodroplets under Rayleigh instability by coupling electrospray with a solgel reaction," *Chemical Physics Letters*, Vol. 445, No. 4, 2007, pp. 271 – 275.

[38]Ichiki, K. and Consta, S., "Disintegration Mechanisms of Charged Aqueous Nanodroplets Studied by Simulations and Analytical Models," *The Journal of Physical Chemistry B*, Vol. 110, No. 39, September 2006, pp. 19168–19175.

[39]Marginean, I., Znamenskiy, V., and Vertes, A., "Charge Reduction in Electrosprays: Slender Nanojets as Intermediates," *The Journal of Physical Chemistry B*, Vol. 110, No. 12, March 2006, pp. 6397–6404.

[40]Giglio, E., Gervais, B., Rangama, J., Manil, B., Huber, B. A., Duft, D., Müller, R., Leisner, T., and Guet, C., "Shape deformations of surface-charged microdroplets," *Physical Review E*, Vol. 77, March 2008, pp. 036319.

[41]Constantopoulos, T. L., Jackson, G. S., and Enke, C. G., "Challenges in achieving a fundamental model for ESI," *Analytica Chimica Acta*, Vol. 406, No. 1, February 2000, pp. 37 – 52.

[42]Dole, M., Mack, L. L., Hines, R. L., Mobley, R. C., Ferguson, L. D., and Alice, M. B., "Molecular Beams of Macroions," *The Journal of Chemical Physics*, Vol. 49, No. 5, 1968, pp. 2240–2249.

[43]Rayleigh, L., "XX. On the equilibrium of liquid conducting masses charged with electricity," *Philosophical Magazine*, Vol. 14, No. 87, 1882, pp. 184–186.

[44]Iribarne, J. V. and Thomson, B. A., "On the evaporation of small ions from charged droplets," *The Journal of Chemical Physics*, Vol. 64, No. 6, 1976, pp. 2287–2294.

[45]Gabelica, V. and Pauw, E. D., "Internal energy and fragmentation of ions produced in electrospray sources," *Mass Spectrometry Reviews*, Vol. 24, No. 4, 2005, pp. 566–587.

[46]Mehta, N. A. and Levin, D. A., "Molecular Dynamics Electrospray Simulations of coarse-grained Ethylammonium Nitrate (EAN) and 1-ethyl-3-methylimidazolium Tetrafluoroborate (EMIM-BF_4)," *Aerospace*, under review.

[47]Plimpton, S., "Fast Parallel Algorithms for Short-Range Molecular Dynamics," *Journal of Computational Physics*, Vol. 117, No. 1, March 1995, pp. 1–19.

[48]Saad, Y. and Schultz, M. H., "GMRES: A Generalized Minimal Residual Algorithm for Solving Nonsymmetric Linear Systems," *SIAM Journal of Scientific and Statistical Computing*, Vol. 7, No. 3, 1986, pp. 856–869.

[49]Lozano, P. C., *Studies on the ion-droplet mixed regime in colloid thrusters*, Ph.D. thesis, Massachusetts Institute of Technology, Department of Aeronautics and Astronautics, 2003.

[50]de la Mora, J. F., "Electrospray ionization of large multiply charged species proceeds via Doles charged residue mechanism," *Analytica Chimica Acta*, Vol. 406, No. 1, February 2000, pp. 93 – 104.

[51]Martino, W., de la Mora, J. F., Yoshida, Y., Saito, G., and Wilkes, J., "Surface tension measurements of highly conducting ionic liquids," *Green Chemistry*, Vol. 8, No. 4, January 2006, pp. 390–397.

[52]Wenhua, G., Heil, P. E., Choi, H., and Kim, K., "Comprehensive model for fine Coulomb fission of liquid droplets charged to Rayleigh limit," *Applied Physics Letters*, Vol. 91, No. 6, August 2007, pp. 064104–1.

[53]Singh, T. and Kumar, A., "Static Dielectric Constant of Room Temperature Ionic Liquids: Internal Pressure and Cohesive Energy Density Approach," *The Journal of Physical Chemistry B*, Vol. 112, No. 41, 2008, pp. 12968–12972.